NANO LETTERS

Letter

pubs.acs.org/NanoLett

Nanoscale Imaging of Local Few-Femtosecond Near-Field Dynamics within a Single Plasmonic Nanoantenna

Erik Mårsell,[†] Arthur Losquin,[†] Robin Svärd,[†] Miguel Miranda,[†] Chen Guo,[†] Anne Harth,[†] Eleonora Lorek,[†] Johan Mauritsson,[†] Cord L. Arnold,[†] Hongxing Xu,[†,‡] Anne L'Huillier,[†] and Anders Mikkelsen*[,†]

[†]Department of Physics, Lund University, P.O. Box 118, 221 00 Lund, Sweden

[‡]School of Physics and Technology, and Institute for Advanced Studies, Wuhan University, Wuhan 430072, China

Supporting Information

ABSTRACT: The local enhancement of few-cycle laser pulses by plasmonic nanostructures opens up for spatiotemporal control of optical interactions on a nanometer and few-femtosecond scale. However, spatially resolved characterization of few-cycle plasmon dynamics poses a major challenge due to the extreme length and time scales involved. In this Letter, we experimentally demonstrate local variations in the dynamics during the few strongest cycles of plasmon-enhanced fields within individual rice-shaped silver nanoparticles. This was done using 5.5 fs laser pulses in an interferometric time-resolved photoemission electron microscopy setup. The experiments are supported by finite-difference time-domain simulations of similar silver structures. The observed differences in the field dynamics across a single particle do not reflect differences in plasmon resonance frequency or dephasing time. They instead arise from a combination of retardation effects and the coherent superposition between multiple plasmon modes of the particle, inherent to a few-cycle pulse excitation. The ability to detect and predict local variations in the few-femtosecond time evolution of multimode coherent plasmon excitations in rationally synthesized nanoparticles can be used in the tailoring of nanostructures for ultrafast and nonlinear plasmonics.

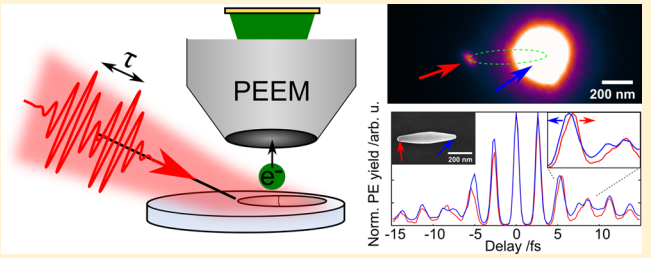

KEYWORDS: *ITR-PEEM, ultrafast plasmonics, optical antennas, multipolar surface plasmons, nanorice, surface plasmon retardation*

Optical antennas made from noble metals such as gold and silver have proven useful in many applications due to their localized surface plasmon (LSP) resonances that can concentrate and alter electromagnetic fields on a nanometer scale.[1−7] Recently, nanoscale optical antennas have been combined with femtosecond laser excitation in the field of ultrafast nano-optics.[8−11] Because of the femtosecond dynamics of the LSP modes, the excitation of optical antennas by ultrashort pulses provides an efficient way to manipulate electromagnetic fields on a nanometer length scale and femtosecond time scale. Manipulating the near-field by changing the excitation pulse, which is an example of coherent control, offers new possibilities to steer nonlinear interactions with light.[12−18] Coherent control of the near-field in an arbitrary system is achieved by selectively exciting a number of eigenmodes of the system with combined amplitude and phase control.[12,16] Especially interesting is the use of few-cycle laser pulses, which provide the bandwidth required to excite many eigenmodes and open up the new regime of few-cycle plasmonics.[12,19−21] However, understanding the complex interplay between different eigenmodes and the optical excitation field in few-cycle plasmonics poses a major challenge due to the extremely short length- and time scales involved. To understand this and to eventually reach full coherent control of the near-field it is crucial to develop characterization methods for imaging the nanolocalized few-femtosecond near-field dynamics resulting from the interaction of broadband plasmonic nanosystems with a few-cycle excitation pulse. An important step in this direction is the measurement of nanoscale variations of the few-cycle near-field dynamics in simple geometric shapes that can be theoretically modeled.

Experimental characterization of optical antennas has been performed using a variety of methods, such as far-field optical spectroscopy,[4,22−24] nonlinear optical spectroscopy,[9,25−27] fast electron spectroscopies,[28−30] photon-induced near-field electron microscopy,[31] scanning near-field optical microscopy,[32,33] and photoemission electron microscopy (PEEM).[15,34−42] Most of these methods have their spatiotemporal resolution limited either by the diffraction of light or by the duration of electron pulses and can thus not characterize near-fields on their natural nanometer and femtosecond scale. However, PEEM circumvents these limitations by combining optical excitation with electron detection, thus getting its temporal resolution from light pulses and its spatial resolution from electron optics.

Received: June 15, 2015
Revised: September 11, 2015
Published: September 16, 2015

DOI: 10.1021/acs.nanolett.5b02363
Nano Lett. 2015, 15, 6601−6608

PEEM imaging of electrons emitted through nonlinear photoemission induced by two identical femtosecond pulses with a phase-stable delay is commonly referred to as interferometric time-resolved PEEM (ITR-PEEM).[36−39] In ITR-PEEM, the local photoemission yield depends on the time-integrated coherent superposition of the local near-fields induced by the two laser pulses. For each pixel in an ITR-PEEM image series, the photoemission yield as a function of delay corresponds to a local nonlinear autocorrelation of the near-field induced by the laser pulse. Of the rapidly increasing number of time-resolved PEEM studies, most have utilized laser pulses of 30 fs duration and upward[35,37,38] with a few studies using shorter pulses down to approximately 10 fs duration.[36,39,43] However, decreasing the pulse duration further can extend the technique to image the complicated few-femtosecond (few-fs) dynamics in broadband plasmonic nanosystems excited by a few-cycle laser pulse. Characterizing the dynamics of localized few-cycle near-fields can be used as input for tailoring novel nanostructures for optimum field control, with applications in ultrafast and nonlinear plasmonics,[20] including harmonic generation,[8,18,27] electron acceleration,[19,21,44] and Raman spectroscopy.[45]

In this work, we used an ITR-PEEM setup with unprecedented temporal resolution to image local variations in the few-fs near-field dynamics within single nanoparticles. The temporal resolution was achieved by using broadband few-cycle laser pulses of 5.5 fs duration, which to our knowledge are the shortest employed in an ITR-PEEM setup. This allowed us to experimentally characterize the local dynamics of few-cycle near-fields and thereby extend the existing ITR-PEEM technique to the regime of few-cycle plasmonics.[19,21,26] As a model system, we studied single rice-shaped Ag nanoparticles, whose simple geometry offers a more thorough understanding of the underlying plasmon dynamics than, for example, studies of field enhancement by random surface roughness.[36] In our experiments, the multiphoton photoemission from different parts of single nanoparticles was measured as a function of delay between two 5.5 fs laser pulses. We observed shifts of the resulting interference fringes between the two ends of a single nanoparticle already at delays of ∼3 fs. These local differences of the near-field autocorrelation trace occurring at few-fs delays is due to a locally varying instantaneous frequency during the few cycles of highest near-field amplitude. This interpretation is confirmed by finite-difference time-domain simulations, which also show that the locally different dynamics arise from a combination of retardation effects and the coherent superposition of multiple LSP modes. This is in contrast to previous ITR-PEEM studies, where differences in the autocorrelation traces were only detected at absolute delays of more than 10 fs and were attributed to different resonance frequencies or dephasing times of the plasmon modes.[36,39] Instead, the local frequency difference detected in our experiments is an inherent effect of the few-cycle pulse excitation giving rise to qualitatively new local near-field dynamics. By imaging frequency variations of the few-cycle plasmon fields within single model nanoparticles, our experiments more generally push the characterization of arbitrarily complex nano-optical systems closer to the ultimate point of experimentally determining local impulse response functions of the system.[46] The improved spatiotemporal characterization is in turn important for reaching full coherent control of optical near-fields on a nanometer and femtosecond scale.

The experiments were performed using a commercial PEEM together with a broadband Ti:sapphire oscillator delivering 5.5 fs laser pulses centered around 800 nm at a repetition rate of 80 MHz. The laser pulse characteristics (see Supporting Information, Figure S1) were monitored using the d-scan technique[47] in a separate characterization arm of the optical setup. The laser pulses impinged on the sample with a 65° incidence angle (see Figure 1a for a sketch of the geometry of the experiment). Our samples consisted of rationally synthesized rice-shaped silver nanoparticles[23,24,48,49] with lengths of 320−600 nm and diameter of ∼100 nm on an indium tin oxide substrate. The particles are good as model systems due to their almost spheroidal geometry, their smooth surfaces, and their lack of crystal grain boundaries. Individual Ag nanoparticles were identified in the PEEM using a Hg discharge lamp, which yields topographic and work function contrast through one-photon photoemission (Figure 1c), and the same particles were afterward imaged using scanning electron microscopy (SEM) (Figure 1b). When the sample was illuminated by p-polarized laser pulses, photoemission was still observed, but only from the nanoparticle ends due to localized field enhancements (Figure 1d,e). The nanoparticle with vertical orientation in Figure 1 is not visible in the multiphoton PEEM image, as its longitudinal LSP modes cannot be excited by p-polarized light. For particles with an angle of maximum 45° to the plane of incidence (which is horizontal in the displayed PEEM images), we detected photoelectrons from one or both ends of the nanoparticle. The laser beam is incident from the left in Figure 1 and all other PEEM images presented in this paper. The ratio of intensities between the two ends varied greatly between particles with the end farthest from the

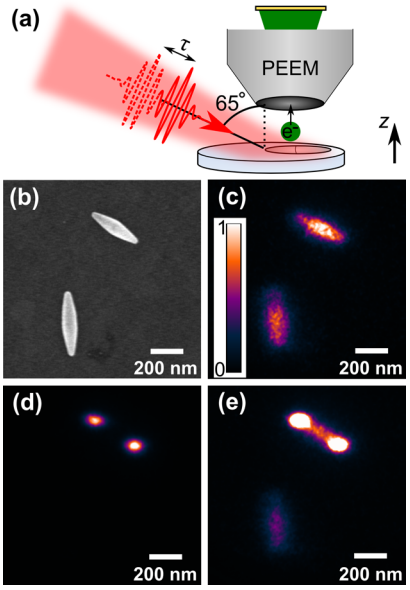

Figure 1. (a) Schematic of the ITR-PEEM experiment with p-polarized laser pulses coming in at a 65° incidence angle. (b) SEM image of two rice-shaped Ag nanoparticles. (c) PEEM image of the same area, acquired using the Hg discharge lamp (one-photon photoemission). (d) PEEM image of the same area, acquired using single p-polarized laser pulses, that is, using only one arm of the interferometer. (e) PEEM image acquired using both the Hg lamp and p-polarized laser pulses. The laser-induced photoemission clearly originates from the two ends of the nanoparticle. The laser beam is incident from the left.

DOI: 10.1021/acs.nanolett.5b02363
Nano Lett. 2015, 15, 6601−6608

laser source always giving a stronger photoemission signal, which is consistent with previous studies,[39,41,50] and reproduced by finite-difference time-domain (FDTD) simulations, as will be shown later. PEEM images of more particles are shown as Supporting Information (Figure S4). By varying the incident laser power, we determined the effective order of the nonlinear photoemission process to be approximately 3.5 (see Supporting Information, Figure S1), which is in accordance with previous studies[39] and indicates that 3 to 4 photons are absorbed for each emitted electron. For simplicity, we will from now on assume the photoemission to be a three-photon process.

As a demonstration of the temporal resolution of our setup, we measured the photoemission yield from two different particles as a function of delay between two identical 5.5 fs laser pulses. The two particles were located 2−3 μm away from each other on the surface, as seen in Figure 2a. This spatial

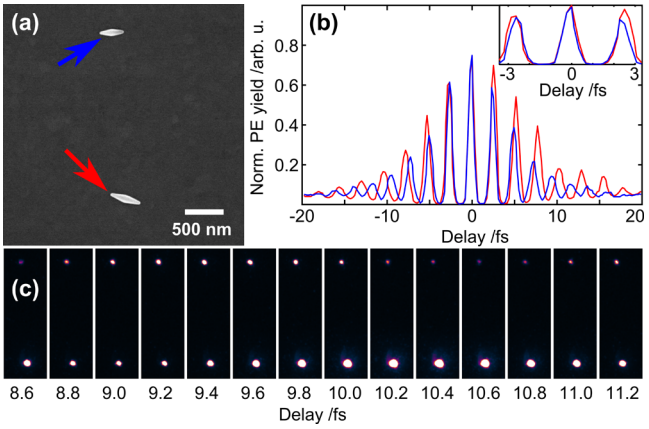

Figure 2. (a) SEM image of two individual Ag nanoparticles, marked by blue (upper) and red (lower) arrows. (b) Normalized near-field autocorrelation traces from the two particles, color coded according to the arrows in (a). A slight shift can be seen already at a phase delay of 2π (see inset for magnification), and at a phase delay of 10π (12−13 fs) the two curves are completely out of phase. The width of the autocorrelation trace from the lower spot (red curve) is artificially large due to a slight saturation of a small fraction (~5% at the peaks at $\pm 2\pi$ delay) of the pixels making up the hot spot on the detector. (c) Frames from the time series, shown on a logarithmic scale.

separation is large enough to hinder near-field coupling between the particles, but small enough to ensure identical wavefronts of the laser pulses. For both of these particles, the photoemission signal was dominated by one end. Frames from an ITR-PEEM scan of these particles show how the spots oscillate out of phase (Figure 2c). The near-field autocorrelation traces from the two particles were obtained by measuring the local photoelectron yield as a function of the delay between two identical pulses and are shown in Figure 2b. The photoelectron yield as a function of delay can, assuming a three-photon process, be estimated as $Y(\vec{r},\tau) \propto \int |\vec{E}(\vec{r},t) + \vec{E}(\vec{r},t+\tau)|^6 \, dt$, where $\vec{E}(\vec{r},t)$ is the local electric field at the surface induced by a single laser pulse.[51] The near-field autocorrelation traces show a difference in oscillation frequency, which is in accordance with other studies of separated nanosystems.[39,43] However, in our experiments the shift between the two curves is visible already at 2π (2.6 fs) delay (see inset of Figure 2b). In previous ITR-PEEM studies, near-field autocorrelation traces from different parts of the sample have all been in phase during at least the first three cycles.[36,39,43] The shift of the peak at 2π delay means that we are probing the particle response in real-time on a sub-3 fs time scale, which is made possible by the use of such short pulses. In this case, the previously used distinction between a region of optical interference due to overlapping pulses and a region of pure light-plasmon interference[36,39,43] is no longer applicable. Instead, differences in the near-field autocorrelation trace are observed at delays where the signal is dominated by interference between the maximum amplitude parts of the induced electric fields. During these few cycles, the plasmon field and the excitation pulse both contribute to the total field at the surface. The difference between the near-field autocorrelation traces from the two particles can be explained by an approximately 10% lower oscillation frequency of the near-field at the larger particle, which in this case is consistent with the expected shift in resonance frequency of the different multipolar resonances for corresponding nanorice lengths (320 and 410 nm, respectively).[24]

Having established the state-of-the-art temporal resolution offered by the use of few-cycle laser pulses in ITR-PEEM, we now turn to studying the near-field dynamics within a single nanosystem. An isolated nanoparticle (380 nm long) for which photoemission from both ends can be detected is shown in Figure 3a. ITR-PEEM images of the same particle for six different delays are shown in Figure 3c−h, showing how the maximum emission shifts from the close end (c−d) to the far end (g−h). The near-field autocorrelation traces from the two

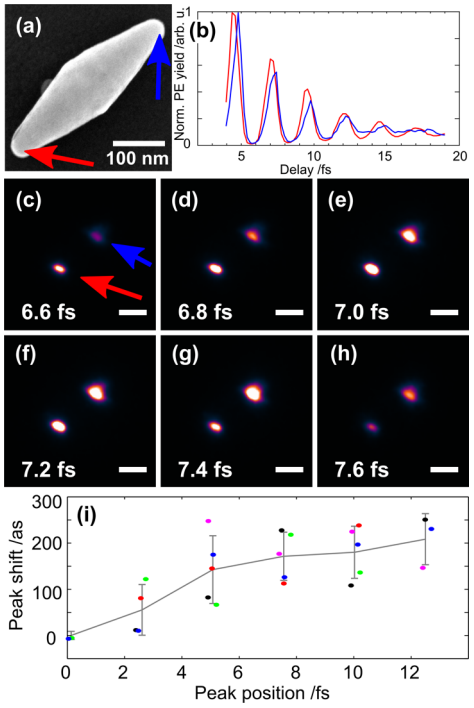

Figure 3. (a) SEM image of an investigated nanoparticle. (b) Parts of the normalized near-field autocorrelation traces measured from the two ends of the nanoparticle in (a). (c−h) Six images of the nanoparticle, acquired with different delays (step size 200 as). Note how in (c−d), the lower left spot is brighter, but in (g−h), the right part is brighter. Scalebars are 200 nm. (i) Extracted peak shifts between the two ends for five separate measurements (each represented by its own color) as a function of delay. Positive peak shift means that the peak from the end farthest from the excitation source is shifted to longer delays. Solid line with error bars: calculated mean and standard deviation of the peak shift for each position.

DOI: 10.1021/acs.nanolett.5b02363
Nano Lett. 2015, 15, 6601−6608

ends of the particle are shown in Figure 3b. The oscillation of the photoemission signal from the end farthest from the excitation is shifted toward longer delays compared to the closest end in the region of 5−15 fs delay. The near-field autocorrelation measurement was repeated several times, and the peak positions were extracted using a local polynomial fitting routine. Peak positions extracted from five separate measurements of the same nanoparticle show that there is a detectable peak shift already at 2π delay, and that it stays approximately constant at around 200 as for delays of 5−15 fs (Figure 3i). Data for five additional particles are shown as Supporting Information, Figure S4. As opposed to the shift between the two different particles, we never observe that the near-field autocorrelation traces from the two ends of a single particle go completely out of phase. This is because of an important distinction; in contrast to the near-fields at two separated particles, the near-field enhancements at the two ends of a single particle result from the same LSP mode(s). As a result, the near-fields at two ends of a single particle are always coupled, and the shift of the autocorrelation trace cannot be interpreted as due to different resonance frequencies of plasmonic normal modes. However, the near-fields at the two ends can still oscillate with slightly different instantaneous frequencies, as evident by the peak shifts in the measured near-field autocorrelation traces.

The shifts of the first few peaks of the near-field autocorrelation traces shown in Figure 3 can be explained by plasmon retardation resulting from the phase variation of the excitation field across the nanoparticle.[37,39,50] Using such an interpretation, we would expect the shifts to be qualitatively similar for different particles but to differ in magnitude depending on the length and the angle of the particle since these parameters determine the phase difference. However, such trends are not observed, suggesting that retardation alone cannot explain the observed shifts for all particles. An example is shown for a longer (490 nm) particle in Figure 4, where first of all a small shift to shorter delays is observed for the photoemission from the end farthest from the excitation at a delay of ±5 fs. Note that this shift is in the opposite direction compared with the particle of Figure 3. Furthermore, both ends exhibit a complicated and slightly different double-peak feature at ±8 fs delay, as labeled by the black arrows. Such a double-peak feature can be explained by the excitation of a coherent superposition of multiple LSP modes, resulting in beating. Control measurements of near-field autocorrelation traces from a nearby region show no sign of this double-peak feature, confirming that the complicated near-field dynamics arises from the nanoparticle itself and not from any irregularities in the temporal structure of the laser pulse (see Supporting Information Figure S2). These complex characteristics of the near-field autocorrelation trace cannot be understood directly from the phase variation of the excitation field across the nanoparticle. Instead they arise from the excitation of multiple LSP modes. When both even and odd LSP modes are excited, their coherent superposition exhibits qualitatively different dynamics at the two ends. Retardation and excitation of multiple modes with different parities can together explain the experimentally observed local differences in the near-field dynamics for all particles in our study.

The interpretation of the experimental observations can be confirmed and better understood by finite-difference time-domain (FDTD) simulations. First, we focus the analysis on the different LSP modes supported by the nanoparticles. Depending on the excitation geometry, both even (m = 2,4,...) and odd (m = 1,3,...) longitudinal modes can be excited within the optical and near-infrared parts of the spectrum.[24,49,52] Even modes are not associated with a net dipole moment and therefore cannot radiate into the far-field in the normal direction. These modes are thus commonly referred to as "dark" (odd modes are correspondingly called "bright").[53] We expect excitation of a mixture of even and odd modes in our experiment due to the grazing incidence geometry in combination with the large bandwidth of the laser pulses. The detected signal then depends on the time-integrated local surface electric field, which is in turn dictated by the coherent superposition of the fields of each excited LSP mode and of the excitation pulse itself. We focus the discussion on the surface electric field response of the particle, which could be seen as a superposition of the plasmon field and the excitation field. This electric field is also what we extract from the FDTD simulations. FDTD modeling of the optical absorption cross-section for particles of 350, 500, and 600 nm length shows that one or two modes can be excited within the spectral bandwidth of the laser (Figure 5a). As expected, the resonances associated with each mode shift to lower frequencies for the longer particles. According to the simulations, the quadrupolar (m = 2) mode overlaps with the laser spectrum for all nanoparticle lengths studied here. The m = 1 and m = 3 modes overlap with the laser spectrum for the shortest and longest particles, respectively. For some particles, such as the 500 nm particle in Figure 5a, we expect the m = 2 mode to dominate the response completely. For the longest particle (600 nm) in the simulation, the m = 2 and m = 3 modes overlap with the laser spectrum (Figure 5a). The corresponding field distributions are shown in Figure 5b,c. To emphasize the different parities of the two modes, we display the projection of the electric field onto the z-axis, that is, the normal to the substrate. To estimate the photoelectron yield from this particle, we calculate the time-

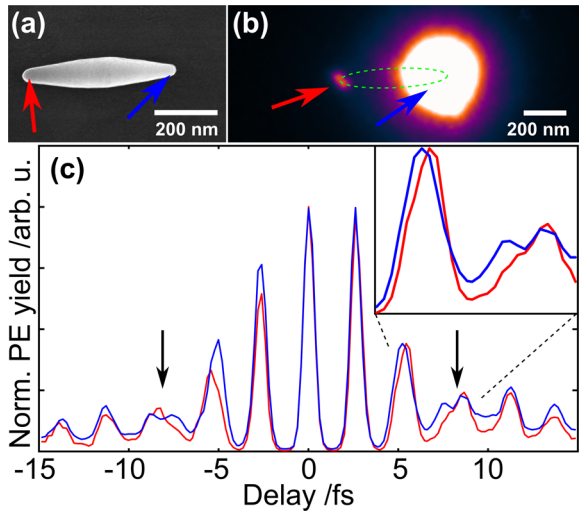

Figure 4. (a) SEM image of an investigated nanoparticle. (b) Multiphoton PEEM image of the same particle. The dashed green line is added to mark the approximate position of the nanoparticle. (c) Near-field autocorrelation traces from the two ends of the particle. The shift of the peak at ±5 fs is in the opposite direction compared to the shift for the particle in Figure 3 with the end farther from the excitation source being shifted to shorter delays. Furthermore, there is a slight difference in the structure of the double peak around ±8 fs (marked with arrows). The inset shows a magnification of this region of the autocorrelation trace (at positive delays).

DOI: 10.1021/acs.nanolett.5b02363
Nano Lett. 2015, 15, 6601−6608

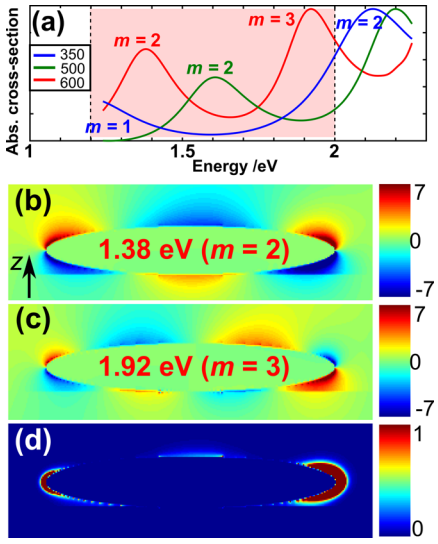

Figure 5. FDTD simulations of the electric field around nanoparticles with 100 nm diameter on a glass substrate, excited by a broadband pulse incident from the left at a 65° incidence angle. For simplicity, the nanoparticle long-axis is set lying in the plane of incidence. (a) Normalized optical absorption spectra for particles of three different lengths, indicated in nanometers in the legend. The red shaded area indicates the approximate spectral window of the laser. Depending on the size, either one or two LSP modes overlap with the laser spectrum. (b) Calculated z-component of the steady-state electric field in the plane of incidence for the m = 2 mode of a 600 nm nanoparticle. (c) Calculated z-component of the steady-state electric field in the plane of incidence for the m = 3 mode of a 600 nm nanoparticle. The colorbars in (b,c) show the field amplitude normalized to the peak amplitude of the excitation pulse. Both modes are almost radially symmetric, except for a slight substrate influence visible in the bottom part of the images. (d) Calculation of $\int |\vec{E}(\vec{r},t)|^6 \, dt$ (normalized to 1) in the plane of incidence, showing an estimate of the photoemission yield from different parts of the particle.

integrated sixth power of the norm of the electric field ($\int |\vec{E}(\vec{r},t)|^6 \, dt$) for each point in the plane of incidence (Figure 5d). See Supporting Information for a detailed discussion on the assumptions of the photoemission process. The modeling shows that we can expect the photoemission signal from the end farther away from the excitation source to be the strongest, and the photoemission from the middle of the particle to be negligible. This relation is valid for all simulated particle sizes. The FDTD simulations thus confirm the features of the experimental images.

To understand the observed local differences in the near-field dynamics, we extracted the time-domain electric field from the FDTD simulations. As examples, we consider one particle (500 nm, left panel of Figure 6) for which the m = 2 mode dominates the simulated response, and one particle (600 nm, right panel of Figure 6) for which both the m = 2 and m = 3 modes contribute. The z-components of the electric field at the end closest to (red curve) and farthest from (blue curve) the laser source are shown as functions of time for the 500 nm particle in Figure 6a. The fields at the two ends are seen to oscillate slightly out of phase during the first few cycles, to later be completely in phase. This can be interpreted as a retardation during the buildup of the excitation, and a free oscillation of the m = 2 LSP mode at a later stage. Since the m = 2 mode is even (see Figure 5b), both ends eventually oscillate in phase. As the fields at the two ends go from oscillating out-of-phase to in-

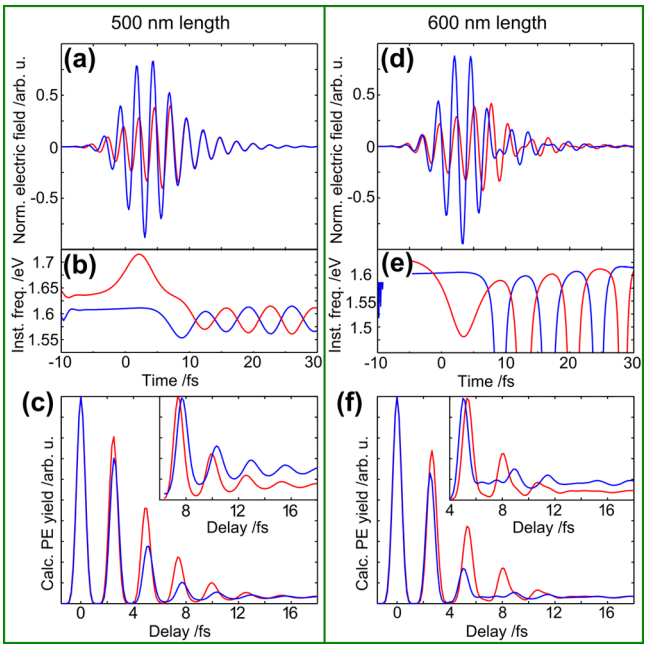

Figure 6. (a) FDTD simulation results showing the z-component of the electric field at the two ends of a nanoparticle of 500 nm length, lying in the plane of incidence, as a function of time. (b) Instantaneous frequencies extracted from the fields in (a). During the few cycles of strongest near-fields, there is a clear difference in the instantaneous frequency. For times >10 fs, the weak fields in combination with numerical errors give rise to an artificial oscillatory behavior of the instantaneous frequency. (c) Normalized near-field autocorrelation traces calculated from the fields in (a). (d) Simulated electric fields for a nanoparticle of 600 nm length. (e) Instantaneous frequencies extracted from the fields in (d). Again, there is a clear difference in the instantaneous frequency around the peak of the near-field. At a later time, the beating between the two excited plasmon modes gives rise to singularities in the instantaneous frequency. (f) Normalized near-field autocorrelation traces calculated from the fields in (d). The insets of panels (c,f) show parts of the same traces normalized differently for easier visualization of the peak shifts.

phase, the net result is a difference in the oscillation frequency. This also means that the frequency difference is inherent to the very short excitation pulse, as the transition from out-of-phase to in-phase occurs during a time dictated by the pulse duration. The instantaneous frequencies of the fields are extracted from the FDTD simulations and shown in Figure 6b. During the few cycles of maximum near-field amplitude, there is a distinct difference in the instantaneous frequency at the two ends. Finally, the third order interferometric autocorrelation traces can be calculated from the simulated fields (Figure 6c). The traces from the two ends of this example particle exhibit a shift similar to that observed in Figure 3. Note also that the shift increases for the first few peaks to then stay approximately constant for delays of more than 10 fs. Comparing to the instantaneous frequency (Figure 6b), we see that the increasing peak shift for delays of 0−10 fs is due to a difference in instantaneous frequency during the few cycles of maximum near-field amplitude. At longer delays, the peak shift does not grow larger, because the difference in instantaneous frequency only exists during a few cycles before the laser pulse has passed and the LSP oscillates freely in the m = 2 eigenmode with both ends in phase.

The other example particle, shown in the right panel of Figure 6, shows more complicated dynamics. The near-fields at

DOI: 10.1021/acs.nanolett.5b02363
Nano Lett. 2015, 15, 6601−6608

the two ends are never in phase, as seen in Figure 6d. This is due to the excitation of two different modes, whose coherent superposition exhibits a beating that is different at the two ends due to the different parities of the $m = 2$ and $m = 3$ modes. For this specific particle, the beating between the two modes results in an instantaneous frequency around the maximum of the field amplitude that is lower for the end close to the excitation (Figure 6e, red curve). Correspondingly, the shift of the first few peaks in the simulated near-field autocorrelation trace (Figure 6e) is in the opposite direction compared to the shorter example particle. For longer delays, the near-field autocorrelation traces show new features reflecting the complicated field dynamics of Figure 6d. Comparing the results from the FDTD simulations with the experiments presented in Figure 3 (Figure 4), we conclude that the shift to larger (smaller) delays of the peaks in the near-field autocorrelation trace corresponds to a lower (higher) instantaneous frequency around the maximum of the near-field at the end farthest from the excitation. Furthermore, the excitation of multiple LSP modes results in a generally more complicated near-field autocorrelation trace. We note that in comparing the experiments and simulations the nanoparticle length giving rise to a specific type of dynamics differs. This discrepancy can be explained by an ∼15% difference in the eigenfrequencies of the modes between experiment and simulation, corresponding to the resonance shift between the nanoparticles of 500 and 600 nm length (see Figure 5a). However, both experiments and simulations show that for some particles, the locally different near-field dynamics can be explained by retardation effects, while for other (longer) particles, the more complicated dynamics arise due to the excitation of multiple LSP modes. The simulations therefore confirm the two different mechanisms for locally different near-field dynamics within single plasmonic nanoparticles with simple shapes: retardation and superposition of even and odd modes.

Many studies have shown the applicability of nanoplasmonic systems to enhance nonlinear processes due to the concentration of light on a nanometer and femtosecond scale. However, to reach full coherent control of the local plasmonic fields, novel characterization methods need to be developed that can measure the localized fields on their natural length- and time scales. Within the new research area of ultrafast and nonlinear plasmonics, the dynamics of enhanced few-cycle plasmonic fields is of particular interest.[19−21,26,44] We have shown that few-cycle pulses can be used in an interferometric time-resolved photoemission electron microscopy setup to characterize such fields by measuring local near-field autocorrelations with ∼3 fs, ∼50 nm resolution. Applying this method to the study of single rice-shaped Ag nanoparticles, we detected local differences in the instantaneous frequency of the enhanced near-field across a single nanoparticle of simple shape. This difference arises although the field enhancement at the two ends of the subwavelength nanoparticle is governed by the same mode(s). The difference therefore cannot be interpreted as due to different resonance frequencies of different plasmon modes, which has been the interpretation in previous ITR-PEEM studies.[36,39] Another major difference compared to previous studies is that we detect differences at much smaller absolute delays, corresponding to differences in the dynamics of the surface electric field during the few cycles of highest amplitude. In previous studies using longer pulses, focus has been on the plasmonic field oscillating at its resonance frequency after the excitation pulse has passed. While this gives valuable, yet narrow-band, information on the sample response, the region of highest amplitude is what dominates the response in applications involving enhancement of nonlinear signals. These new observations fully result from the few-cycle duration of the exciting laser pulses. Although the exact reconstruction of the local near-field dynamics from the autocorrelation traces is not possible, we claim that local near-field autocorrelation using few-cycle laser pulses in ITR-PEEM is currently the most powerful method for spatiotemporal characterization of plasmonic fields. This is due to the broad spectral range and well-defined time structure of the excitation in combination with the nanometer spatial resolution. In the future, PEEM experiments using an infrared pump pulse and an extreme ultraviolet attosecond probe pulse are expected to give a more direct measurement of the plasmonic near-field than the near-field autocorrelation can provide.[54−57] However, in this work we show how ITR-PEEM using few-cycle pulses can reveal locally different few-fs dynamics within a single nanoparticle of simple shape. These experiments on well-defined model nanoparticles can be generalized to plasmonic systems of arbitrary complexity, ranging from tailored multi-resonant nanoantennas[7,18] to random disordered systems.[12,16]

In summary, we have combined ITR-PEEM with 5.5 fs laser pulses to locally map the ultrafast temporal evolution of enhanced few-cycle electric fields within silver rice-shaped model nanoantennas. The use of unprecedentedly short pulses allows us to probe differences in the dynamics of the local near-field during the few cycles of highest amplitude. We find that the asymmetric excitation leads to locally different ultrafast near-field dynamics across a single nanoparticle. In particular, the instantaneous frequency during the few cycles of strongest oscillation is shown to be different at different points of the nanoparticle, despite the plasmonic field being driven by the same modes. The differences are inherent to the few-cycle excitation and can be understood by the combination of two effects: plasmon retardation due to phase variations of the excitation field across the nanoparticle, together with the coherent superposition of even and odd plasmon modes. This is to our knowledge the first experimental demonstration of how these two effects can translate into a frequency difference of the few-cycle plasmon field across a single subwavelength nanoparticle. This has implications for any use of plasmonic systems to enhance few-cycle pulses, and especially for boosting nonlinear effects such as harmonic generation or electron emission. Such applications are extremely sensitive to the detailed few-cycle near-field dynamics when the field is the strongest, dynamics that has up until now been inaccessible for nanometer-resolved characterization methods.

Methods. The experimental setup was based on a broadband oscillator (VENTEON Pulse One) delivering pulses of 5.5 fs duration, 800 nm central wavelength, and 250 pJ pulse energy at a repetition rate of 80 MHz. Double-chirped mirrors and a pair of glass wedges were used for dispersion compensation to achieve the optimal pulse duration on the sample. The pulse was sent through a properly calibrated, compact Michelson interferometer with a piezo mirror enabling a range of delays between −250 fs and +250 fs in steps of 67 as. The beam was then focused by a 20 cm focal length achromat lens onto the sample surface at an angle of 65° to the surface normal. The resulting focal spot dimensions were approximately $50 \times 100\ \mu m^2$ on the sample. After the interferometer, a flip mirror could send the beam to a separate arm for pulse characterization. In this separate pulse characterization arm, the

DOI: 10.1021/acs.nanolett.5b02363
Nano Lett. 2015, 15, 6601−6608

beam passed through a window identical to the entrance window of the PEEM chamber and was focused by an identical lens into a thin BBO crystal for second harmonic generation. By measuring the second harmonic spectrum as a function of glass thickness in the beam, the pulse could be completely characterized using the d-scan technique.[47]

To obtain the experimental near-field autocorrelation trace, the images were first drift compensated using an automatic hot-spot tracking routine. Then, the intensity in the area of the spot was measured from each image and a background intensity measured from a featureless area was subtracted. The resulting near-field autocorrelation trace was subjected to a narrow Gaussian smoothing filter (σ = 60 as).

The samples consisted of polyol-synthesized rice-shaped Ag nanoparticles[48] that were drop-cast from ethanol solution onto substrates of ITO on glass. The samples were directly transferred into a ultrahigh vacuum chamber with a base pressure of 10^{-9} mbar. After the PEEM measurements, the samples were studied in a scanning electron microscope (Hitachi SU8010).

Finite-difference time-domain modeling was performed using the commercial software FDTD Solutions from Lumerical. The Ag nanoparticles were modeled as ellipsoidal particles with a dielectric function taken from literature,[58] lying on a fused silica substrate. A staircase-type mesh with a minimum element size of 2.5 nm was used. The calculations were performed with a broadband modulated Gaussian total field scattered field plane wave source. The excitation spectral range was set to match the actual laser spectrum covered by the experiment. The simulation space was closed with Perfectly Matched Layers. Frequency-dependent quantities, such as absorption cross-section and field patterns, were obtained through Fourier transform and normalization by the excitation.

■ ASSOCIATED CONTENT

Supporting Information

The Supporting Information is available free of charge on the ACS Publications website at DOI: 10.1021/acs.nanolett.5b02363.

Supplementary figures and their descriptions and detailed discussions about the photoemission modeling and the interpretation of the experiments. (PDF)

■ AUTHOR INFORMATION

Corresponding Author

*E-mail: anders.mikkelsen@sljus.lu.se.

Notes

The authors declare no competing financial interest.

■ ACKNOWLEDGMENTS

This work was supported by NanoLund, the Swedish Research Council (VR), the Swedish Foundation for Strategic Research (SSF), the Crafoord Foundation, the Knut and Alice Wallenberg Foundation, and the European Research Council (ERC) (startup grant ElectronOpera and advanced grant PALP).

■ REFERENCES

(1) Wessel, J. *J. Opt. Soc. Am. B* **1985**, *2*, 1538−1541.
(2) Mühlschlegel, P.; Eisler, H.-J.; Martin, O. J. F.; Hecht, B.; Pohl, D. W. *Science* **2005**, *308*, 1607−1609.
(3) Xia, Y.; Halas, N. J. *MRS Bull.* **2005**, *30*, 338−348.
(4) Wiley, B.; Sun, Y.; Xia, Y. *Acc. Chem. Res.* **2007**, *40*, 1067−1076.
(5) Novotny, L.; van Hulst, N. *Nat. Photonics* **2011**, *5*, 83−90.
(6) Knight, M. W.; Sobhani, H.; Nordlander, P.; Halas, N. J. *Science* **2011**, *332*, 702−704.
(7) Celebrano, M.; Wu, X.; Baselli, M.; Gromann, S.; Biagioni, P.; Locatelli, A.; De Angelis, C.; Cerullo, G.; Osellame, R.; Hecht, B.; Du, L.; Ciccacci, F.; Finazzi, M. *Nat. Nanotechnol.* **2015**, *10*, 412−417.
(8) Kim, S.; Jin, J.; Kim, Y.-J.; Park, I.-Y.; Kim, Y.; Kim, S.-W. *Nature* **2008**, *453*, 757−760.
(9) Anderson, A.; Deryckx, K. S.; Xu, X. G.; Steinmeyer, G.; Raschke, M. B. *Nano Lett.* **2010**, *10*, 2519−2524.
(10) Hanke, T.; Cesar, J.; Knittel, V.; Trgler, A.; Hohenester, U.; Leitenstorfer, A.; Bratschitsch, R. *Nano Lett.* **2012**, *12*, 992−996.
(11) Schumacher, T.; Kratzer, K.; Molnar, D.; Hentschel, M.; Giessen, H.; Lippitz, M. *Nat. Commun.* **2011**, *2*, 333.
(12) Stockman, M. I.; Faleev, S. V.; Bergman, D. J. *Phys. Rev. Lett.* **2002**, *88*, 067402.
(13) Stockman, M. I.; Bergman, D. J.; Kobayashi, T. *Phys. Rev. B: Condens. Matter Mater. Phys.* **2004**, *69*, 054202.
(14) Brixner, T.; García de Abajo, F. J.; Schneider, J.; Spindler, C.; Pfeiffer, W. *Phys. Rev. B: Condens. Matter Mater. Phys.* **2006**, *73*, 125437.
(15) Aeschlimann, M.; Bauer, M.; Bayer, D.; Brixner, T.; Garcia de Abajo, F. J.; Pfeiffer, W.; Rohmer, M.; Spindler, C.; Steeb, F. *Nature* **2007**, *446*, 301−304.
(16) Li, X.; Stockman, M. I. *Phys. Rev. B: Condens. Matter Mater. Phys.* **2008**, *77*, 195109.
(17) Silberberg, Y. *Annu. Rev. Phys. Chem.* **2009**, *60*, 277−292.
(18) Aouani, H.; Navarro-Cia, M.; Rahmani, M.; Sidiropoulos, T. P. H.; Hong, M.; Oulton, R. F.; Maier, S. A. *Nano Lett.* **2012**, *12*, 4997−5002.
(19) Dombi, P.; Irvine, S. E.; Rácz, P.; Lenner, M.; Kroó, N.; Farkas, G.; Mitrofanov, A.; Baltuška, A.; Fuji, T.; Krausz, F.; Elezzabi, A. Y. *Opt. Express* **2010**, *18*, 24206−24212.
(20) Raschke, M. B.; Berweger, S.; Atkin, J. M. In *Plasmonics: Theory and Applications*; Shahbazyan, T. V., Stockman, M. I., Eds.; Challenges and Advances in Computational Chemistry and Physics; Springer: Netherlands, 2013; Vol. *15*; pp 237−281.
(21) Piglosiewicz, B.; Schmidt, S.; Park, D. J.; Vogelsang, J.; Grosz, P.; Manzoni, C.; Farinello, P.; Cerullo, G.; Lienau, C. *Nat. Photonics* **2013**, *8*, 37−42.
(22) Sönnichsen, C.; Franzl, T.; Wilk, T.; von Plessen, G.; Feldmann, J.; Wilson, O.; Mulvaney, P. *Phys. Rev. Lett.* **2002**, *88*, 077402.
(23) Wang, H.; Brandl, D. W.; Le, F.; Nordlander, P.; Halas, N. J. *Nano Lett.* **2006**, *6*, 827−832.
(24) Wei, H.; Reyes-Coronado, A.; Nordlander, P.; Aizpurua, J.; Xu, H. *ACS Nano* **2010**, *4*, 2449−2654.
(25) Lamprecht, B.; Krenn, J. R.; Leitner, A.; Aussenegg, F. R. *Phys. Rev. Lett.* **1999**, *83*, 4421−4424.
(26) Hanke, T.; Krauss, G.; Träutlein, D.; Wild, B.; Bratschitsch, R.; Leitenstorfer, A. *Phys. Rev. Lett.* **2009**, *103*, 257404.
(27) Accanto, N.; Piatkowski, L.; Renger, J.; van Hulst, N. F. *Nano Lett.* **2014**, *14*, 4078−4082.
(28) Powell, C. J.; Swan, J. B. *Phys. Rev.* **1959**, *115*, 869−875.
(29) Kociak, M.; Stephan, O. *Chem. Soc. Rev.* **2014**, *43*, 3865−3883.
(30) Losquin, A.; Zagonel, L. F.; Myroshnychenko, V.; Rodríguez-González, B.; Tencé, M.; Scarabelli, L.; Förstner, J.; Liz-Marzán, L. M.; García de Abajo, F. J.; Stéphan, O.; Kociak, M. *Nano Lett.* **2015**, *15*, 1229−1237.
(31) Barwick, B.; Flannigan, D. J.; Zewail, A. H. *Nature* **2009**, *462*, 902−906.
(32) Fischer, U. C.; Pohl, D. W. *Phys. Rev. Lett.* **1989**, *62*, 458−461.
(33) Onishi, S.; Matsuishi, K.; Oi, J.; Harada, T.; Kusaba, M.; Hirosawa, K.; Kannari, F. *Opt. Express* **2013**, *21*, 26631−26641.
(34) Schmidt, O.; Fecher, G.; Hwu, Y.; Schönhense, G. *Surf. Sci.* **2001**, *482−485*, 687−692.
(35) Schmidt, O.; Bauer, M.; Wiemann, C.; Porath, R.; Scharte, M.; Andreyev, O.; Schönhense, G.; Aeschlimann, M. *Appl. Phys. B: Lasers Opt.* **2002**, *74*, 223−227.

DOI: 10.1021/acs.nanolett.5b02363
Nano Lett. 2015, 15, 6601−6608

(36) Kubo, A.; Onda, K.; Petek, H.; Sun, Z.; Jung, Y. S.; Kim, H. K. *Nano Lett.* **2005**, *5*, 1123−1127.
(37) Bauer, M.; Wiemann, C.; Lange, J.; Bayer, D.; Rohmer, M.; Aeschlimann, M. *Appl. Phys. A: Mater. Sci. Process.* **2007**, *88*, 473−480.
(38) Lemke, C.; Leißner, T.; Evlyukhin, A.; Radke, J. W.; Klick, A.; Fiutowski, J.; Kjelstrup-Hansen, J.; Rubahn, H.-G.; Chichkov, B. N.; Reinhardt, C.; Bauer, M. *Nano Lett.* **2014**, *14*, 2431−2435.
(39) Sun, Q.; Ueno, K.; Yu, H.; Kubo, A.; Matsuo, Y.; Misawa, H. *Light: Sci. Appl.* **2013**, *2*, e118.
(40) Aeschlimann, M.; Brixner, T.; Fischer, A.; Kramer, C.; Melchior, P.; Pfeiffer, W.; Schneider, C.; Strber, C.; Tuchscherer, P.; Voronine, D. V. *Science* **2011**, *333*, 1723−1726.
(41) Douillard, L.; Charra, F.; Korczak, Z.; Bachelot, R.; Kostcheev, S.; Lerondel, G.; Adam, P.-M.; Royer, P. *Nano Lett.* **2008**, *8*, 935−940.
(42) Word, R. C.; Fitzgerald, J.; Könenkamp, R. *Appl. Phys. Lett.* **2011**, *99*, 041106.
(43) Qin, J.; Ji, B.-Y.; Hao, Z.-Q.; Lin, J.-Q. *Chin. Phys. Lett.* **2015**, *32*, 064202.
(44) Dombi, P.; Hörl, A.; Rácz, P.; Márton, I.; Trügler, A.; Krenn, J. R.; Hohenester, U. *Nano Lett.* **2013**, *13*, 674−678.
(45) Moskovits, M. *J. Raman Spectrosc.* **2005**, *36*, 485−496.
(46) Huang, J. S.; Voronine, D. V.; Tuchscherer, P.; Brixner, T.; Hecht, B. *Phys. Rev. B: Condens. Matter Mater. Phys.* **2009**, *79*, 195441.
(47) Miranda, M.; Arnold, C. L.; Fordell, T.; Silva, F.; Alonso, B.; Weigand, R.; L'Huillier, A.; Crespo, H. *Opt. Express* **2012**, *20*, 18732−18743.
(48) Liang, H.; Yang, H.; Wang, W.; Li, J.; Xu, H. *J. Am. Chem. Soc.* **2009**, *131*, 6068−6069.
(49) Liang, H.; Zhao, H.; Rossouw, D.; Wang, W.; Xu, H.; Botton, G. A.; Ma, D. *Chem. Mater.* **2012**, *24*, 2339−2346.
(50) Melchior, P.; Bayer, D.; Schneider, C.; Fischer, A.; Rohmer, M.; Pfeiffer, W.; Aeschlimann, M. *Phys. Rev. B: Condens. Matter Mater. Phys.* **2011**, *83*, 235407.
(51) Aeschlimann, M.; Bauer, M.; Bayer, D.; Brixner, T.; Cunovic, S.; Dimler, F.; Fischer, A.; Pfeiffer, W.; Rohmer, M.; Schneider, C.; Steeb, F.; Strber, C.; Voronine, D. V. *Proc. Natl. Acad. Sci. U. S. A.* **2010**, *107*, 5329−5333.
(52) Zhang, S.; Chen, L.; Huang, Y.; Xu, H. *Nanoscale* **2013**, *5*, 6985−6991.
(53) Nordlander, P.; Oubre, C.; Prodan, E.; Li, K.; Stockman, M. I. *Nano Lett.* **2004**, *4*, 899−903.
(54) Stockman, M. I.; Kling, M. F.; Kleineberg, U.; Krausz, F. *Nat. Photonics* **2007**, *1*, 539−544.
(55) Mikkelsen, A.; Schwenke, J.; Fordell, T.; Luo, G.; Klünder, K.; Hilner, E.; Anttu, N.; Zakharov, A. A.; Lundgren, E.; Mauritsson, J.; Andersen, J. N.; Xu, H. Q.; L'Huillier, A. *Rev. Sci. Instrum.* **2009**, *80*, 123703.
(56) Chew, S. H.; Süßmann, F.; Späth, C.; Wirth, A.; Schmidt, J.; Zherebtsov, S.; Guggenmos, A.; Oelsner, A.; Weber, N.; Kapaldo, J.; Gliserin, A.; Stockman, M. I.; Kling, M. F.; Kleineberg, U. *Appl. Phys. Lett.* **2012**, *100*, 051904.
(57) Mårsell, E.; Arnold, C. L.; Lorek, E.; Guenot, D.; Fordell, T.; Miranda, M.; Mauritsson, J.; Xu, H.; L'Huillier, A.; Mikkelsen, A. *Ann. Phys. (Berlin, Ger.)* **2013**, *525*, 162−170.
(58) Palik, E. D. *Handbook of Optical Constants of Solids*; Academic: London), 1985.

DOI: 10.1021/acs.nanolett.5b02363
Nano Lett. 2015, 15, 6601−6608